Time-resolved Monitoring of Enzyme Activity with Ultrafast Hyper-CEST Spectroscopy

Jörg Döpfert[1], Matthias Schnurr[1], Martin Kunth,[1*] Honor May Rose[1], Andreas Hennig[2], and Leif Schröder[1]

[1]Molecular Imaging, Leibniz-Forschungsinstitut für Molekulare Pharmakologie (FMP), Robert-Rössle-Str. 10, 13125 Berlin, Germany

[2]Department of Life Sciences and Chemistry, Jacobs University Bremen, Campus Ring 1, 28759 Bremen, Germany

*current affiliation: Division of Chemistry and Chemical Engineering, California Institute of Technology, 1200 E California Blvd, Pasadena, CA 91125

E-mail: lschroeder@fmp-berlin.de

Abstract

We propose a method to dynamically monitor the progress of an enzymatic reaction using NMR of hyperpolarized ^{129}Xe in a host-guest system. It is based on a displacement assay originally designed for fluorescence experiments that exploits the competitive binding of the enzymatic product on the one hand and a reporter dye on the other hand to a supramolecular host. Recently, this assay has been successfully transferred to NMR, using xenon as a reporter, cucurbit[6]uril as supramolecular host, and Hyper-CEST as detection technique. Its advantage is that the enzyme acts on the unmodified substrate and only the product is detected through immediate inclusion into the host. We here apply a method that drastically accelerates the acquisition of Hyper-CEST spectra *in vitro* using magnetic field gradients. This allows monitoring the dynamic progress of the conversion of lysine to cadaverine with a temporal resolution of ~30 s. Moreover, the method only requires to sample the very early onset of the reaction (<0.5 % of substrate conversion where the host itself is required only at µM concentrations) at comparatively low reaction rates, thus saving enzyme material and reducing NMR acquisition time. The obtained value for the specific activity agrees well with previously published results from fluorescence assays. We furthermore outline how the Hyper-CEST results correlate with xenon T_2 measurements performed during the enzymatic reaction. This suggests that ultrafast Hyper-CEST spectroscopy can be used for dynamically monitoring enzymatic activity with NMR.

This article has been accepted for publication and undergone full peer review but has not been through the copyediting, typesetting, pagination and proofreading process which may lead to differences between this version and the Version of Record. Please cite this article as doi: 10.1002/mrc.4702

Introduction

The development of methods for the detection of enzymatic activity is of great relevance both for drug discovery and for disease diagnostics in molecular imaging.[1,2] Different options exist for reporting catalyzed substrate conversion. Sufficiently translucent samples allow for optical detection, for example, as introduced by Hennig et al. in terms of a concept of fluorescent supramolecular displacement assays.[3] For opaque samples, NMR is often the method of choice due to its unlimited penetration depth. Its inherent low sensitivity can be circumvented by CEST detection (chemical exchange saturation transfer). This technique uses the presence of a dilute (mM) pool of a CEST agent to encode a loss of signal in an abundant pool. The most common implementation relies on the exchange between bulk water protons and labile ^{1}H sites that are selectively saturated while residing on the CEST agent.[4] Other implementations of the CEST technique made its enhancement also available for X nuclei NMR: these include ^{19}F-labeled CEST probes that undergo a conformational change[5], ^{19}F-labelled hosts in exchanging host-guest systems,[6,7] ^{13}C and ^{15}N NMR applications for sparsely populated protein conformers,[8–11] a ^{15}N MRI reporter,[12] and ^{129}Xe that is transiently bound to a cage-like host structure.[13]

Enzyme activity detection has been addressed in depth by so-called catalyCEST agents introduced by Pagel and co-workers. The common conceptual idea is that the enzyme directly acts on the CEST agent. This can be a paramagnetic chelate[14] or a diamagnetic compound[15,16] in which the nature or number of exchanging proton sites that contribute to the CEST effect is changed through the catalytic reaction. Alternatively, a product cleaved from the agent can turn itself into a CEST-detectable agent and contribute a new signal.[17] Agents have been implemented for detection of various types of enzymes, including esterase,[18] sulfatase,[15,17] transglutaminase,[14] and galactosidase and glucuronidase.[19]

A recent platform approach that was used for several of these examples is based on salicylic acid and includes an enzyme-responsive and an unresponsive CEST site in the substrate of which the unresponsive remains on the product.[16] However, many enzymes have reduced activity when their original substrate is coupled to a reporter such as salicylic acid (a 1170-fold reduction has been reported in ref. [16]). This limitation can be circumvented by introducing a spacer between the actual substrate moiety and the CEST reporter sub-unit. But as observed for the case of β-glucuronidase, the

derivative is not necessarily stable in enzyme-free solution.[19] An approach where the enzyme still acts on the "native" substrate would therefore be clearly favorable.

In this regard, the displacement assay mentioned above has the advantage that the substrate remains unmodified and only the product causes a signal response upon acting itself on an existing host-guest complex. This assay has recently been translated to localized detection of enzymatic activity using xenon NMR imaging.[20] Figure 1 displays the reaction pathways (a) and the analogy of the assays: For fluorescence (b), the sample contains the substrate, a supramolecular host, and a reporter dye. The host readily forms inclusion complexes with the dye, triggering an observable fluorescence change. Upon addition of the enzyme, the substrate is converted into the product, which has a much higher binding affinity for the host than the dye. Therefore, the product immediately displaces the dye from the host, and the fluorescence spectral properties of the dye change. The progress of the enzymatic reaction can then be monitored via an observable gradually changing fluorescence intensity as more and more product is generated.

In the NMR analogy, Schnurr et al.[20] replaced the reporter dye by Xe atoms (see Fig. 1c). In this case, the binding of ^{129}Xe to the host leads to a change in the NMR chemical shift instead of a change in fluorescence. This unique chemical shift of bound Xe (ca. 90 ppm away from the resonance of free dissolved Xe) allows to selectively saturate ^{129}Xe while residing inside the host. Using a cw RF pulse over several seconds, cucurbit[6]uril (CB6) as the host enables a very efficient saturation transfer due to its chemical exchange rates of k_{BA} ~ 2100 s^{-1} into the pool of free Xe in aqueous environment.[21] To allow for the observation of highly dilute concentrations of bound ^{129}Xe, the method combines spin hyperpolarization and CEST (Hyper-CEST[13]) which has already been applied for various other molecular sensing applications.[22–26] Addition of the enzyme for substrate conversion into the product with its high host affinity displaces Xe from the host and thus reduces the Hyper-CEST response, *i.e.* prevents the saturation transfer onto dissolved Xe.

The full potential of the assay, i.e. monitoring the course of the reaction, has not yet been exploited with Xe NMR. We hypothesized that the sensitivity enhancement is of particular benefit for observing the initial reaction rate, v_0, that is typically sought after for characterizing enzyme activity. This is because Hyper-CEST can detect the product already at low concentrations that occur very early on in the reaction. The challenge for CEST measurements is that reliable quantification of the signals that

change over the course of the reaction requires acquisition of entire *z*-spectra, i.e. plotting the observed bulk pool signal intensity vs. the variable frequency offset of the applied saturation pulse. This is rather time consuming and reported temporal resolution for catalyCEST studies ranges between 3.6 min[19] and 7.5 min.[16] Diamagnetic compounds used in those studies also need to be present in mM concentrations to yield a sufficient dynamic range of the CEST responses for quantification over time. catalyCEST data therefore typically relies on substrate concentrations up to 50-60 mM and the reaction time is stretched over several hours by choosing an appropriate enzyme concentration.[16,19] This is necessary to obtain accurate values for v_0. However, the Hyper-CEST approach for the displacement assay now gives the opportunity to assess v_0 from monitoring only the very onset of the reaction as the initially achieved amounts of product are sufficient to acquire a dynamic range for determining d[product]/dt.

The strong focus on the start of the reaction ensures to obtain a linear signal behavior over almost the entire dynamic range (here corresponding to the host concentration of 16 µM) with many data points. This is different from non-displacement fluorescence methods and catalyCEST analysis where the signal approaches a plateau in a non-linear way (see Fig. 1d). According to the Michaelis-Menten model of enzyme kinetics, the product concentration increases linearly with time with maximum rate, v_{max}, determined by the catalytic turnover number ($v_{max} = k_{cat}$ [enzyme]) as long as the remaining substrate concentration is much larger than the Michaelis-Menten constant K_M. When the substrate concentration becomes lower, the reaction rate also decreases until it follows a single exponential decay with a constant characteristic for a pseudo-first-order kinetics reaction of the enzyme catalysis (k_{cat}/K_M) when the substrate concentration is much smaller than K_M. Regardless of the actual conditions, it is common to approximate the initial time frame of the progress curve by a linear behavior to determine the initial rate v_0. [16,19,27]

Though conventional acquisition of *z*-spectra with Hyper-CEST is also not fast due to multiple re-deliveries of hyperpolarized Xe (~10 min for entire spectra), *in vitro* characterization allows to sacrifice one spatial dimension in the NMR setup to encode the spectral dimension in an accelerated way. Adjusting the overall reaction time to ca. 30 min is then sufficient to sample many data points for extracting information about enzyme activity. The detection relies on our recently proposed method to drastically accelerate the acquisition of Hyper-CEST spectra *in vitro* using magnetic

field gradients referred to as ultrafast CEST spectroscopy (UCS).[28] The concept is related to similar techniques that have been used for ^{1}H CEST spectroscopy.[29–31] Here, we employ this method to monitor for the first time the progress of an enzymatic reaction with Xe NMR at a temporal resolution of ~30 s. In particular, we observe the conversion of lysine (Lys) to cadaverine (Cad) induced by the enzyme lysine decarboxylase (LDC), using CB6 as a host for the competitive binding of Xe and Cad. We show how a measure for the product concentration can be obtained from the Hyper-CEST response in the acquired UCS spectra at each time point, allowing us to extract initial reaction rates and to estimate the enzymatic activity. In addition, we show that not only the Hyper-CEST response, but also the apparent T_2 relaxation time of unbound Xe changes in the course of the enzymatic reaction. This parameter then yields reaction rates, too, that are in excellent correlations with the UCS measurements.

Experimental

All MR experiments were performed on a 9.4 T NMR spectrometer (AV 400, Bruker Biospin, Ettlingen, Germany) equipped with gradient coils. A 10 mm inner diameter double-resonant (^{1}H and ^{129}Xe) probe was used for excitation and detection. Hyperpolarized Xe was produced by spin exchange optical pumping (ca. 25% spin polarization after transfer into the NMR spectrometer) in a custom designed continuous flow setup using a gas mixture of 5% Xe (26.4% natural abundance of ^{129}Xe), 10% N_2 and 85% He. Using the pressure from the polarizer (ca. 4.5 atm. abs.), the mix was directly bubbled into a 10 mm NMR tube containing 1.5 ml of the sample solution for 12 s at a total flow rate of 0.14 SLM (standard liter per minute) followed by a 1.5 s delay (to allow the remaining bubbles to collapse) prior to each scan.[32,33]

All samples were initially prepared from a stock solution consisting of CB6 and Lys with concentrations 16 µM and 6 mM, respectively, dissolved in a buffer (10 mM ammonium acetate in H_2O) at pH = 6.0 (the preferred pH condition for optimum LDC activity[3]). To start the enzymatic reaction, LDC (from *Bacillus cadaveris*, 1.6 U/mg) was added, and then the sample was quickly placed inside the NMR spectrometer for data acquisition where it was kept at 25°C. Lys, Cad, and LDC were obtained from Sigma-Aldrich (Steinheim, Germany).

Enzymatic reactions were monitored through ultrafast Hyper-CEST NMR spectra acquired using a turbo spin echo sequence modified for UCS[28] with the following parameters: 64 data points over a CEST bandwidth of 16 kHz (145 ppm) and a readout field of view of L_r =1 cm, cw saturation pulse with B_1 =16 µT and duration 3 s, slice thickness 1.8 cm, echo time 16 ms, echo train length 32, receiver bandwidth 5 kHz, 1 ms Gaussian excitation and refocusing pulses. The acquired spin echoes of each scan were averaged in complex space to increase the signal-to-noise ratio. The resulting average spin echo was Fourier transformed and then its magnitude was taken to obtain a magnetization profile. An ultrafast Hyper-CEST spectrum was obtained by dividing such a profile acquired with a saturation pulse by a profile acquired without saturation pulse.[28] Note that we did not necessarily include all the 32 acquired echoes into the complex averaging operation, but instead an "SNR-optimal" number, that was calculated as described in the Supporting Information of ref. [28]. The spectra were centered around a chemical shift of -91.5 ppm, as this is the expected chemical shift of xenon bound to CB6. All post-processing was performed using python (version 2.7).

Results and Discussion

Monitoring Enzyme Dynamics using ultrafast Hyper-CEST spectroscopy

After addition of the enzyme LDC to the Lys sample at time point t = 0 and its transfer into the NMR magnet, we successively acquired Xe UCS spectra every 34 s to monitor the amount of remaining accessible CB6 hosts – that is, hosts that are not occupied by the product Cad and hence are accessible for xenon during the ongoing enzymatic reaction.

Fig. 2 shows UCS spectra at selected time points t for an enzyme concentration of 5 µg/mL. The spectra clearly show the decrease of the large signal of the observed pool of unbound Xe due to saturation transfer mediated through chemical exchange of ^{129}Xe in and out of the host at the characteristic chemical shift of Xe@CB6 δ = -91.5 ppm (upfield from free Xe in solution) in this buffer solution. The depth of this dip – the CEST response – is directly related to the amount of accessible CB6. The initial spectrum at t = 4.2 min is characterized by such efficient saturation transfer that the overlap with the direct saturation centered at 0 ppm starts to manifest already around

-50 ppm. Fig. 2 shows a reduction of this depth with time: As more and more Cad is produced, it blocks more and more CB6 hosts and thus prevents them from participating in the chemical exchange process for Xe. It is intuitively clear that in the absence of any additional competing guests, the average reaction rate over the production of the initial 16 µM of Cad is determined by the cut-off time elapsed until the first completely flat UCS spectrum is recorded, *i.e.* at $t = t_{off}$. Hence, a simple approximation for v_0 is possible from plotting the CEST intensity over time, identifying t_{off} and assigning $v_0 = 16\ \mu M/t_{off}$. Note that this is easier to identify than the completion of the entire reaction with [substrate]($t_{complete}$) = 0 over the full range of [substrate] = 6 mM. The Xe displacement assay can hence be tailored to truly work in the linear range of enzyme activity. However, instead of guessing t_{off} from the UCS data, an even more accurate evaluation is possible because an entire time course of the [substrate](t) can be obtained to derive v_0 with higher accuracy. We therefore expect the analytical error for the change in the UCS signal to be rather small.

It is possible to derive the concentration of accessible CB6, [$CB6_{acc}$](t), from the UCS spectra. CEST responses follow a certain line shape that can be fitted for quantitative analysis. However, the signal intensity is not linearly related to the concentration of the CEST pool. For catalyCEST, a Lorentzian line shape is used but a calibration curve of %CEST effect vs. [agent] is needed to convert the observed (substrate) signal into a concentration. For Hyper-CEST spectra, an analytical solution comprising exponential Lorentzians has been derived[34] and confirmed experimentally.[35] This allows to directly obtain (product) concentration values from the CEST responses as outlined in the Appendix.

Fig. 3 shows the extracted time course [$CB6_{acc}$](t) during the progress of the reaction for three experiments conducted with three different enzyme concentrations. As expected, [$CB6_{acc}$] decreases highly linearly with time for each experiment until it enters into the noise level, which indicates that all initially available CB6 hosts are occupied with a Cad molecule. Not surprisingly, the noise level is reached the faster the more enzyme is present in the sample and the kink would already be a reasonable guess for t_{off} and v_0. It is noteworthy that because of the low concentration of CB6 relative to the available substrate (16 µM vs. 6 mM), the dynamic range of the data in Fig. 3 represents only 0.26% of the possible substrate conversion. The excellent linear signal change clearly confirms that we monitor only the very beginning of the reaction

where v_0 is constant and does not gradually decrease due to a too rapid substrate conversion.

It should be mentioned that the time courses show larger signal variability at the beginning, an effect that becomes more visible for the slower progressing reaction. The initial data is presumably noisier because Xe-accessible CB7 shortens the T_2 and determines the "SNR-optimal" number of echoes that are used to reconstruct the projection profiles for calculating the UFC spectra. Hence, initial spectra reconstructed from fewer echoes come with a larger variability.

Since each Lys molecule is converted to exactly one Cad molecule during the reaction, and considering that each produced Cad molecule immediately displaces a Xe atom and blocks exactly one CB6 host (quantitative binding[36], $K_a > 10^9$ M^{-1}), the rate of change in [$CB6_{acc}$] (before reaching the noise level) equals the substrate depletion rate -d/dt [Lys] or product growth d/dt [Cad]:

$$\frac{d[\mathrm{Lys}]}{dt} = -\frac{d[\mathrm{Cad}]}{dt} = \frac{d[\mathrm{CB6_{acc}}]}{dt} \quad (1)$$

Data in Fig. 3 was therefore fitted to a linear decrease in which the intersection with the ordinate was forced through the calibration value of 16 µM. The slope then represents v_0. As displayed in Tab. 1, the R^2 values for each fit are close to unity, confirming that the concentrations extracted from the non-linear CEST response indeed follow a linear model. This is an impressive example that quantification of Hyper-CEST data is very straightforward based on the analytical FHC model[34,35] with its simplifications that are not applicable in ^{1}H CEST. Knowing the starting concentration of the Hyper-CEST agent, no further calibration of the CEST response in needed.

The reaction rate v_0 certainly depends on the sample temperature. The high temporal resolution of the UFC method would also allow to study the LDC activity at physiological temperature or a whole set of temperature conditions. Hyper-CEST studies at different temperatures could demonstrate improved sensitivity for T ~ 37°C.[37–39] CEST responses at intermediate time points acquired under different temperature conditions cannot be directly compared since also the Xe solubility changes in a non-linear way with T as does the Xe exchange kinetics. However, the reaction rates derived from the overall progression of the displacement assay (knowing the initial concentration of accessible host) are indeed suitable to compare LDC activity at different temperature conditions.

Plotting v_0 vs. the used enzyme concentration yields a measure for the specific activity (= k_{cat}). The result is shown in Fig. S-1(a). The average value of 75±3 µmol/min/g extracted from the three results in Tab. 1 is insignificantly higher than the previously published value (74 µmol/min/g) for the same enzyme using the fluorescence-based supramolecular assay. The excellent agreement of this value with the fluorescence assay performed by Schnurr et al.[20] suggests that the substrate concentrations applied previously (220 µM) as well as herein (6 mM) are well above the K_M. In that former study, we followed the decrease of 300 µM substrate down to 220 µM (using 80 µM CB6) and could observe very linear plots even for ca. 25% substrate conversion. In view of the much higher substrate concentrations applied and much lower fraction of substrate conversion followed herein, it is thus clear that the initial substrate conversion rate should be linear over the complete observation time.

It is noteworthy that for the system investigated here, there are no significant deviations between the fluorescence assay and the NMR results. As mentioned above, the analytical error must be small and potential errors in reaction rate values that could yield a different activity are presumably dominated by concentration errors for either the host or the enzyme. Fluorescence techniques are usually considered as more precise and deviations of 1-2 orders of magnitude between values for v_{max} derived from NMR and fluorescence have been reported for the salicylic acid platform approach.[19] In fact, the good agreement for both read-outs of the displacement assay actually also represents a confirmation that the displacement step for Xe is not biased over the dye displacement. The fluorescence assay verified that even for enzyme concentrations of 200 µg/ml the produced Cad practically immediately displaces the dye in the host when the latter one is present at ~10^{-5} M.[20] In terms of stability, the association constant K_a of Cad binding to CB6 in NH_4OAc buffer is ca. 10^9 – 10^{10} M^{-1} vs. K_a = 4×10^4 M^{-1} for the dye. For the Xe NMR assay, exchange kinetics of Cad inclusion have not been quantified in the presence of dissolved Xe, but the good agreement of the results confirms that binding of the monoatomic gas to CB6 appears to be labile enough that any increase in product concentration directly triggers an immediate and persistent 1:1 displacement event.[a]

[a] Association of supramolecular host-guest complexes is commonly very fast and often even diffusion-limited (see for example: 10.1021/jacs.7b04821 and *J. Am. Chem. Soc.* **1999**, *121*, 8022-8032). Using the diffusion limit in water as maximum association rate constant (7.4 x 10^9 $M^{-1}s^{-1}$) and K_a = 10^9 M^{-1} as a lower estimate for the binding constant, allows to assess the dissociation rate constant as $k_d = k_a/K_a$ < 7.4 s^{-1}. In consequence,

formation of the Cad@CB6 complex is much faster than enzymatic conversion and the complex is very persistent with respect to Xe exchange.

This article has been accepted for publication and undergone full peer review but has not been through the copyediting, typesetting, pagination and proofreading process which may lead to differences between this version and the Version of Record. Please cite this article as doi: 10.1002/mrc.4702

We can therefore draw three conclusions: First, the inclusion of Cad in the presence of "competing" Xe is not a rate limiting step for the overall signal cascade into the reduced CEST response and the enzyme reaction itself (quantified by k_{cat}) dominates the time scale. Second, this fast displacement practically establishes a new equilibrium that warrants the assumptions in the Appendix for linking the maximum CEST response (λ_{max}) and the pool size of bound Xe (f). Third, a sufficiently high affinity K_a of Cad@CB6 is retained in the reaction mixture (as previously reported[20,36]), which excludes that a biased low amount of product formation that would not fully translate as a loss in CEST signal. Particularly the last point was highly expected because the $K_a \sim 2.5 \times 10^3$ reported[21] for Xe@CB6 is even lower than that of the dye.

It should be mentioned that Lys binds into CB6 at high concentrations (K_a = 880 M^{-1} for lysine in 10 mM Tris, pH 7.5, M. Nilam, A. Hennig, unpublished results) as observed by Xe NMR in ref. [20]. However, this should not significantly influence the quantitative results for the displacement assays (neither fluorescence nor NMR) since only a very small fraction of the starting substrate concentration might be associated with the much more dilute host as recently shown for a related fluorescence-based ornithine decarboxylase assay.[27]

Correlation of [$CB6_{acc}$] with the observed apparent T_2

It is well-known that chemical exchange has an effect on the measured apparent T_2 relaxation time (which manifests as exchange line broadening in conventional spectra).[40] With regard to our experimental setup, when residing inside a CB6 host, Xe experiences a different chemical shift than if it is unbound in solution. Hence, during signal acquisition after NMR excitation, the Xe atoms accumulate different phase shifts according to their individual residence times in CB6, resulting in a loss of phase coherence and hence a shortening of the observed apparent T_2 decay. We can therefore assume that Xe in CB6 solution shows a relative short T_2 at the beginning of the displacement progress. Essential is the following (linear) decrease of the host concentration that reduces the exchange-mediated relaxation contribution and hence to a gradual prolongation of the apparent relaxation decay. The $T_{2,app}$ times were extracted from the spin echoes of the UCS scans, as described in the Supporting Information, S-2. Figure 4 shows the results of repeated $T_{2,app}$ measurements (every 34 s) from the echo train analysis during the enzymatic reaction for three different

enzyme concentrations. The loss in [$CB6_{acc}$] causes a hyperbolic increase in $T_{2,app}$ until we observe an expected plateau which reflects the "true" T_2 of Xe in the sample solution.

It is interesting to note that contrary to Fig. 3, the final data in Fig. 4 is noisier than at the beginning of the time course. Data in Fig. 4 is extracted from a train of 32 echoes with an echo distance of 16 ms. Hence, this covers the transverse signal decay over ca. 0.5 s. This is sufficient to quantify the exponential decay when T_2 is short, i.e. at the beginning of the reaction where initial values are less than 300 ms. As the reaction progresses and T_2 increases, the 0.5 s time window yields less precise results for relaxation analysis. This is particularly true for the final points where the effective relaxation time approaches 1.3 s.

We analyzed the time courses $T_{2,app}(t)$ through their second derivative to identify the time point for the kink in the curve. To reduce noise in the derivative, the time course data was smoothed by an adjacent average filter of window size 3. This still yields a good agreement of the kink position of the solid line plot with the scattered data points. The time for $(d/dt)^2\ T_{2,app} = 0$ was determined with Origin's intersection gadget as shown in Fig. S-3. This corresponds to the cut-off time, t_{off}, for using up 16 µM of initially accessible CB6 and thus yields reaction rates are shown in Tab. 1. Plotting these v_0 values vs. the used enzyme concentrations (see Fig. S-1(a)) shows that the derived activity of 75±2 µmol/min/g agrees perfectly with the value obtained above by UCS and also with the fluorescence assay results. The correlation between the T_2-derived reaction rate data and the CEST-related values is shown in Fig. S-1 (b) and demonstrates that the slope is practically 1.

We could thus demonstrate a strong correlation between the CEST measurement and the $T_{2,app}$ measurement. However, the fact that the UCS spectra directly enable us to estimate the substrate concentration at every instant until all CB6 is occupied renders CEST analysis preferable against the T_2 measurements for the task of monitoring enzymatic activity: data in the fit for the CEST signal strength contributes equally along the dynamic range due to the linear behavior and thus helps to improve the accuracy. The T_2 curve, however, is mainly analyzed in a rather short time window around the cut-off time. The data points representing the dominant part of the dynamic range are not truly considered and the accuracy might be reduced compared to the CEST evaluation that models data over a larger time window.

Conclusion

In this work, we demonstrated for the first time the dynamic monitoring of an enzymatic reaction using Xe Hyper-CEST. Our results for the decarboxylation of lysine show excellent agreement with results from fluorescence-based experiments, demonstrating the feasibility of the method *in vitro*. This suggests that UCS can be used as an alternative approach for quantifying certain enzymatic activities in opaque or turbid samples where fluorescence detection is challenging. It should also be useful in the context of recently developed rotaxane probes for enzyme detection.[41] These are compounds where the enzyme acts on the axle part to change a CEST response from the macrocycle like CB6 around the axle.

The temporal resolution of ~30 s that is sufficient to sample many time points at the onset of the reaction with constant reaction rate is enabled by fast signal acquisition with UCS. Because this requires scarifying one spatial dimension to encode the spectral information, transition to CEST imaging of a non-isotropic object requires modification of the approach. However, our group and others have developed tools where accelerated CEST acquisition can be obtained from more complex samples than the one used here,[42] including *in vivo* applications.[43] It should be mentioned in this context that fast CEST spectroscopy techniques, in particular the *in vitro* protocols,[29,30,42] could also be used to facilitate catalyCEST agent development.

The UFC method in the presented form quantifies enzyme kinetics less comprehensive than conventional Michaelis-Menten kinetics. However, the method should also be applicable to a set of variable concentrations of the substrate and therefore be suitable to derive v_{max}, K_M, and related parameters. For fluorescence-based assays of this type, a complete enzymatic characterization including determination of k_{cat}, K_M, as well as inhibition modes and constants were recently demonstrated.[27] Regarding applications in more complex environments, all CEST methods face the challenge that a single signal is not sufficient for quantification when the local concentration is not known. Recent implementations for catalyCEST therefore include an enzyme-responsive and an unresponsive signal,[44] where a very elegant approach combines these two signals in one reporter.[16,19] This eliminates concentration-dependent effects that distort quantification. Localized activity maps representing the reaction coordinate of the entire enzymatic reaction (instead of absolute values in µM/min) as one signal changes while the other remains constant

can then be obtained *in vivo*.[16] Such an approach could also be feasible for the NMR displacement assay when combining a host such as CB6 for competitive binding with a second one that is not receptive for the product of the reaction. Cryptophanes have been used by many groups for Xe NMR and bind Xe stable in various environments.[45–48] They could serve as the non-responsive CEST site to implement a ratiometric approach in which progress along the reaction coordinate of the displacement reaction (which is a small fraction of the enzymatic reaction) is used to derive activity maps. Related cucurbit[n]urils have already been tested for *in vivo* applications in the context of drug delivery containers,[49–52] hence the synthesis of a "tandem host" should be considered. The results presented here might thus be of great use for the development of new molecular sensing and imaging applications for Hyper-CEST displacement assays, including localized detection enzymatic activity, as proposed by Schnurr et al.[20]

Appendix:

Estimation of the accessible CB6 concentration from the UCS spectra

In a first step, we show that *f*, the ratio between the concentration of xenon atoms inside the host and the concentration of unbound xenon atoms, is proportional to the concentration of Cad-accessible CB6 hosts [$CB6_{acc}$]. Then, we illustrate how *f* can be estimated from the measured ultrafast Hyper-CEST spectra. Finally, the absolute [$CB6_{acc}$] can be obtained by normalization to the known initial CB6 concentration.

We model the chemical inclusion complex formation of xenon and CB6 with the following reversible reaction

$$\mathrm{Xe@sol} + \mathrm{CB6_{empty}} \leftrightarrow \mathrm{Xe@CB6} \tag{2}$$

where Xe@sol denotes unbound xenon in solution, $CB6_{empty}$ denotes empty CB6 hosts (i.e. not occupied by xenon nor by Cad) and Xe@CB6 denotes xenon bound to CB6. With this notation, the above-mentioned ratio *f* reads

$$f = \frac{[\mathrm{Xe@CB6}]}{[\mathrm{Xe@sol}]} \tag{3}$$

and the equilibrium constant is given by

$$K_a = \frac{[\mathrm{Xe@CB6}]}{[\mathrm{Xe@sol}][\mathrm{CB6_{empty}}]} \tag{4}$$

where all concentrations are equilibrium concentrations. Using these equations, and assuming that one CB6 molecule can accommodate exactly one xenon atom at a time, the total concentration of CB6 cages accessible for newly produced Cad adds up to

$$\begin{aligned}[\mathrm{CB6_{acc}}] &= [\mathrm{Xe@CB6}] + [\mathrm{CB6_{empty}}] \\ &= f[\mathrm{Xe@sol}] + \frac{1}{K_a}\frac{[\mathrm{Xe@CB6}]}{[\mathrm{Xe@sol}]} \\ &= f\left([Xe@sol] + \frac{1}{K_a}\right) \end{aligned} \quad (5)$$

Hence, [CB6$_{acc}$] and f are directly linked through a proportionality factor: K_a is constant by definition, and [Xe@sol] can be regarded as constant, too, as we saturate the sample solution with dissolved xenon for each measurement and therefore [Xe@sol] is given by xenon's Ostwald solubility in that solution.[35]

Next, we illustrate how a quantity proportional to f can be obtained from the UCS spectra shown in Fig. 2. According to Zaiss et al.,[34] the shape of a Hyper-CEST spectrum can be modeled by an analytical function

$$z(\delta\omega) = M_0 e^{-\lambda_{\mathrm{depol}}(\delta\omega)t_{\mathrm{sat}}} \quad (6)$$

where $\delta\omega$ is the saturation frequency, M_0 is the initial xenon magnetization prior to the application of the saturation pulse, t_{sat} is the duration of the saturation pulse and λ_{depol} is a Lorentzian line shape (plus a constant C)

$$\lambda_{\mathrm{depol}} = \frac{\lambda_{\max}\frac{\Gamma^2}{4}}{\frac{\Gamma^2}{4} + (\delta\omega - \delta\omega_0)^2} + C \quad (7)$$

with amplitude λ_{max}, width Γ, and center $\delta\omega_0$ (corresponding to the resonance frequency of xenon inside CB6). The constant C depends on relaxation rates and the tilt angle of the effective B_1 field, and cancels out upon normalization, as described below. In Eq. (7), λ_{max} is the parameter of interest as it can be approximated as being proportional to the forward exchange rate, k_a, of Xe binding into CB6 (see Eq. (15) in ref. [34] when the frequency separation of the saturated and the observed pool is large compared to the transverse relaxivity, R_2, the backward exchange rate, k_b, and the saturation strength in Hz, ω_1). Critically, k_a itself is proportional to f due to the rate equation in steady state (Eq. (2) in ref [34]). Assuming for now, that the high affinity for CB6 of any produced Cad is linked to a sufficiently fast reach of a new equilibrium seen by Xe, λ_{max} is directly proportional to f.

We therefore determine the intensity z_{min} of the UCS spectra at their minimum, i.e. at maximum saturation $\delta\omega = \delta\omega_0$. Since all our UCS spectra are normalized through the division by a reference scan without saturation,[28] both the constant C in Eq. (7) and M_0 in Eq. (6) cancel out, yielding

$$z_{\min} = z(\delta\omega = \delta\omega_0) = e^{-\lambda_{\max} t_{\text{sat}}} \tag{8}$$

As the negative logarithm of this expression

$$-\log z_{\min} = \lambda_{\max} t_{\text{sat}} \tag{9}$$

is proportional to λ_{max}, we successfully found a quantity that is proportional to $[CB6_{acc}]$:

$$-\log z_{\min} \propto \lambda_{\max} \propto f \propto [CB6_{\text{acc}}] \tag{10}$$

In practice, we extracted z_{min} from each measured UCS spectrum at time point t by integrating the spectra in a small interval containing three data points around their minima. The integration boundaries are represented by the dotted lines in Fig. 2. To obtain a scaling for the absolute concentration $[CB6_{acc}](t)$ as depicted in Fig. 3, we linearly extrapolated the time curves $-\log(z_{min}(t))$ to $t = 0$, and normalized these curves such that the extrapolation intersected the y-axis at the known initial concentration of accessible CB6, *i.e.*, $[CB6_{acc}](t = 0) = 16$ µM.

Acknowledgments

Nils Bogdanoff is gratefully acknowledged for assisting with data processing. This work was supported by the European Research Council under the European Community's Seventh Framework Programme (FP7/2007-2013)/ERC grant agreement no. 242710 and funding SCHR 995/5-1 from the German Research Foundation to L.S. as well as funding HE 5967/4-1 from the German Research Foundation to A.H.

References

(1) Goddard, J.-P.; Reymond, J.-L. *Curr. Opin. Biotechnol.* **2004**, *15* (4), 314.
(2) Weber, W. A.; Czernin, J.; Phelps, M. E.; Herschman, H. R. *Nat. Clin. Pract. Oncol.* **2008**, *5* (1), 44.
(3) Hennig, A.; Bakirci, H.; Nau, W. M. *Nat. Methods* **2007**, *4* (8), 629.
(4) Yoo, B.; Raam, M. S.; Rosenblum, R. M.; Pagel, M. D. *Contrast Media Mol. Imaging* **2007**, *2* (4), 189.
(5) Bar-Shir, A.; Gilad, A. A.; Chan, K. W. Y.; Liu, G.; van Zijl, P. C. M.; Bulte, J. W. M.; McMahon, M. T. *J. Am. Chem. Soc.* **2013**, *135* (33), 12164.
(6) Avram, L.; Iron, M. A.; Bar-Shir, A. *Chem Sci* **2016**.
(7) Avram, L.; Wishard, A. D.; Gibb, B. C.; Bar-Shir, A. *Angew. Chem. Int. Ed.* **2017**.
(8) Sekhar, A.; Kay, L. E. *Proc. Natl. Acad. Sci.* **2013**, *110* (32), 12867.
(9) Vallurupalli, P.; Bouvignies, G.; Kay, L. E. *J. Am. Chem. Soc.* **2012**, *134* (19), 8148.
(10) Vallurupalli, P.; Kay, L. E. *Angew. Chem. Int. Ed.* **2013**, *52* (15), 4156.
(11) Bouvignies, G.; Vallurupalli, P.; Kay, L. E. *J. Mol. Biol.* **2014**, *426* (3), 763.
(12) Zeng, H.; Xu, J.; Yadav, N. N.; McMahon, M. T.; Harden, B.; Frueh, D.; van Zijl, P. C. M. *J. Am. Chem. Soc.* **2016**, *138* (35), 11136.
(13) Schroder, L.; Lowery, T. J.; Hilty, C.; Wemmer, D. E.; Pines, A. *Science* **2006**, *314* (5798), 446.
(14) Hingorani, D. V.; Randtke, E. A.; Pagel, M. D. *J. Am. Chem. Soc.* **2013**, *135* (17), 6396.
(15) Sinharay, S.; Fernández-Cuervo, G.; Acfalle, J. P.; Pagel, M. D. *Chem. – Eur. J.* **2016**, *22* (19), 6491.
(16) Sinharay, S.; Randtke, E. A.; Jones, K. M.; Howison, C. M.; Chambers, S. K.; Kobayashi, H.; Pagel, M. D. *Magn. Reson. Med.* **2017**, *77* (5), 2005.
(17) Fernández-Cuervo, G.; Sinharay, S.; Pagel, M. D. *ChemBioChem* **2016**, *17* (5), 383.
(18) Li, Y.; Sheth, V. R.; Liu, G.; Pagel, M. D. *Contrast Media Mol. Imaging* **2011**, *6* (4), 219.
(19) Fernández-Cuervo, G.; Tucker, K. A.; Malm, S. W.; Jones, K. M.; Pagel, M. D. *Bioconjug. Chem.* **2016**, *27* (10), 2549.
(20) Schnurr, M.; Sloniec-Myszk, J.; Döpfert, J.; Schröder, L.; Hennig, A. *Angew. Chem. Int. Ed.* **2015**, *54* (45), 13444.
(21) Kunth, M.; Witte, C.; Hennig, A.; Schröder, L. *Chem. Sci.* **2015**, *6* (11), 6069.
(22) Shapiro, M. G.; Ramirez, R. M.; Sperling, L. J.; Sun, G.; Sun, J.; Pines, A.; Schaffer, D. V.; Bajaj, V. S. *Nat. Chem.* **2014**, *6* (7), 629.
(23) Schnurr, M.; Sydow, K.; Rose, H. M.; Dathe, M.; Schröder, L. *Adv. Healthc. Mater.* **2015**, *4* (1), 40.
(24) Rose, H. M.; Witte, C.; Rossella, F.; Klippel, S.; Freund, C.; Schröder, L. *Proc. Natl. Acad. Sci.* **2014**, *111* (32), 11697.
(25) Witte, C.; Martos, V.; Rose, H. M.; Reinke, S.; Klippel, S.; Schröder, L.; Hackenberger, C. P. R. *Angew. Chem. Int. Ed.* **2015**, *54* (9), 2806.
(26) Piontek, A.; Witte, C.; May Rose, H.; Eichner, M.; Protze, J.; Krause, G.; Piontek, J.; Schröder, L. *Ann. N. Y. Acad. Sci.* **2017**, *1397* (1), 195.
(27) Nilam, M.; Gribbon, P.; Reinshagen, J.; Cordts, K.; Schwedhelm, E.; Nau, W. M.; Hennig, A. *SLAS Discov. Adv. Life Sci. RD* **2017**, 2472555216689288.
(28) Döpfert, J.; Witte, C.; Schröder, L. *ChemPhysChem* **2014**, *15* (2), 261.
(29) Xu, X.; Lee, J.-S.; Jerschow, A. *Angew. Chem. Int. Ed Engl.* **2013**, *52* (32), 8281.
(30) Döpfert, J.; Witte, C.; Schröder, L. *J. Magn. Reson.* **2013**, *237*, 34.
(31) Boutin, C.; Léonce, E.; Brotin, T.; Jerschow, A.; Berthault, P. *J. Phys. Chem. Lett.* **2013**, *4* (23), 4172.
(32) Witte, C.; Kunth, M.; Döpfert, J.; Rossella, F.; Schröder, L. *J. Vis. Exp.* **2012**, No. 67.
(33) Lakshmanan, A.; Lu, G. J.; Farhadi, A.; Nety, S. P.; Kunth, M.; Lee-Gosselin, A.; Maresca, D.; Bourdeau, R. W.; Yin, M.; Yan, J.; Witte, C.; Malounda, D.; Foster, F. S.; Schröder, L.; Shapiro, M. G. *Nat. Protoc.* **2017**, *12* (10), 2050.

(34) Zaiss, M.; Schnurr, M.; Bachert, P. *J. Chem. Phys.* **2012**, *136* (14), 144106.
(35) Kunth, M.; Witte, C.; Schröder, L. *J. Chem. Phys.* **2014**, *141* (19), 194202.
(36) Praetorius, A.; Bailey, D. M.; Schwarzlose, T.; Nau, W. M. *Org. Lett.* **2008**, *10* (18), 4089.
(37) Schröder, L.; Meldrum, T.; Smith, M.; Lowery, T.; Wemmer, D.; Pines, A. *Phys. Rev. Lett.* **2008**, *100* (25).
(38) Schröder, L.; Chavez, L.; Meldrum, T.; Smith, M.; Lowery, T. J.; Wemmer, D. E.; Pines, A. *Angew. Chem. Int. Ed.* **2008**, *47* (23), 4316.
(39) Schilling, F.; Schröder, L.; Palaniappan, K. K.; Zapf, S.; Wemmer, D. E.; Pines, A. *ChemPhysChem* **2010**, *11* (16), 3529.
(40) Bain, A. D. *Prog. Nucl. Magn. Reson. Spectrosc.* **2003**, *43* (3), 63.
(41) Slack, C.; Finbloom, J. A.; Jeong, K.; Bruns, C. J.; Wemmer, D. E.; Pines, A.; Francis, M. B. *Chem Commun* **2016**.
(42) Döpfert, J.; Zaiss, M.; Witte, C.; Schröder, L. *J. Magn. Reson.* **2014**, *243*, 47.
(43) Liu, Z.; Dimitrov, I. E.; Lenkinski, R. E.; Hajibeigi, A.; Vinogradov, E. *Magn. Reson. Med.* **2016**, *75* (5), 1875.
(44) Yoo, B.; Sheth, V. R.; Howison, C. M.; Douglas, M. J. K.; Pineda, C. T.; Maine, E. A.; Baker, A. F.; Pagel, M. D. *Magn. Reson. Med.* **2014**, *71* (3), 1221.
(45) Schröder, L. *Phys. Med.* **2013**, *29* (1), 3.
(46) Wang, Y.; Dmochowski, I. J. *Acc. Chem. Res.* **2016**, *49* (10), 2179.
(47) Mari, E.; Berthault, P. *Analyst* **2017**.
(48) Palaniappan, K. K.; Francis, M. B.; Pines, A.; Wemmer, D. E. *Isr. J. Chem.* **2014**, *54* (1–2), 104.
(49) Montes-Navajas, P.; González-Béjar, M.; Scaiano, J. C.; García, H. *Photochem. Photobiol. Sci.* **2009**, *8* (12), 1743.
(50) Uzunova, V. D.; Cullinane, C.; Brix, K.; Nau, W. M.; Day, A. I. *Org. Biomol. Chem.* **2010**, *8* (9), 2037.
(51) Chen, H.; Chan, J. Y. W.; Yang, X.; Wyman, I. W.; Bardelang, D.; Macartney, D. H.; Lee, S. M. Y.; Wang, R. *RSC Adv* **2015**, *5* (38), 30067.
(52) Hettiarachchi, G.; Nguyen, D.; Wu, J.; Lucas, D.; Ma, D.; Isaacs, L.; Briken, V. *PLoS ONE* **2010**, *5* (5), e10514.

Table 1: Initial reaction rate v_0 for different LDC concentrations using a CB6 concentration of 16 µM. Values are either obtained by linearly fitting the data in Fig. 3 or from cut-off times t_{off} analyzing T_2 data in Fig. 4.

[LDC] [µg/mL]; [nM]*	v_0 [nM/min]	R^2	t_{off} [min]	v_0 [nM/min]
5; 62	439	0.989	37.35	428
10; 123	765	0.977	21.39	748
15; 185	1099	0.980	14.49	1104

*Note: Estimation of an upper limit for the concentration using MW = 81 kDa and assuming a 100% pure product.

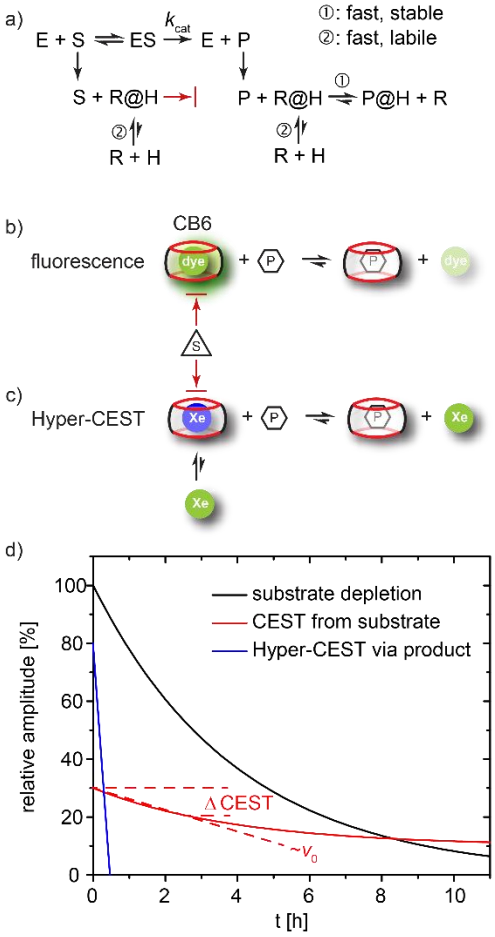

Fig. 1: Principle of displacements assays for detecting enzymatic activity. **(a)** Involved reaction pathways: the enzyme (E) acts on the substrate (S) to produce the product (P). S does not replace the reporter (R) from the host (H). The product, however, has a very high affinity for H and displaces R to form a stable inclusion complex. The inclusion reactions are fast on the time scale of the catalytic reaction governed by k_{cat}. **(b)** Displacement of the dye from the host by the product leads to a fluorescence decrease. **(c)** Displacement of Xe from the host by the product interrupts the chemical exchange needed for saturation transfer between caged and free Xe. Critically, Xe has different resonance frequencies depending on the molecular environment (represented by different colors). **(d)** Signal dynamics for different CEST approaches while the substrate is depleted over hours (following a pseudo-first order reaction illustrated by the black line): CEST effects from a diamagnetic agent that acts as a substrate usually amount to only a small fraction of the initial bulk pool signal (here: 30 %) and do not necessarily vanish completely (illustrated by the red solid line). The reaction needs to be followed for a long time to observe a significant change Δ CEST (horizontal dashed lines for starting and end signal) which allows to derive an approximated v_0 (slope of the diagonal dashed line). The Hyper-CEST detection via displacement through the product starts with a strong saturation transfer amplitude (> 50%, blue line) and has a large dynamic range with linear, complete disappearance within a short time.

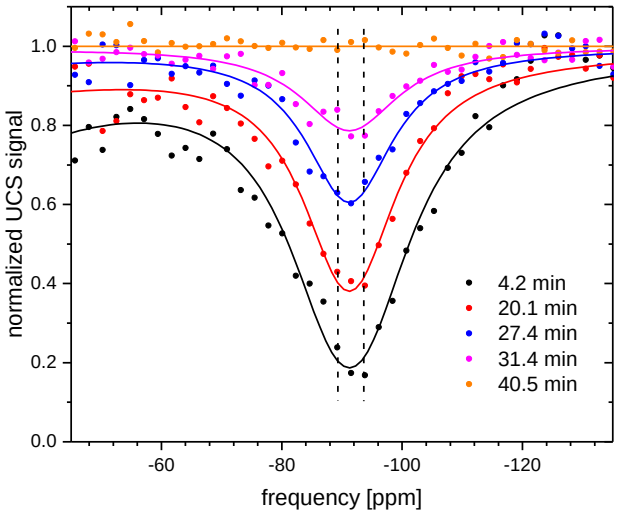

Fig. 2: Ultrafast Hyper-CEST spectra for selected time points after the beginning of the enzymatic reaction using an LDC concentration of 5 µg/mL. The solid lines were obtained by fitting the data to Eq. (6)/(7). The dotted lines indicate the range of integration to obtain the minimum of the spectrum, as described in the Appendix. Note that from all acquired 64 data points, only the central 44 are shown, since the remaining exhibited a high noise level due to the restricted sample geometry.[29,30]

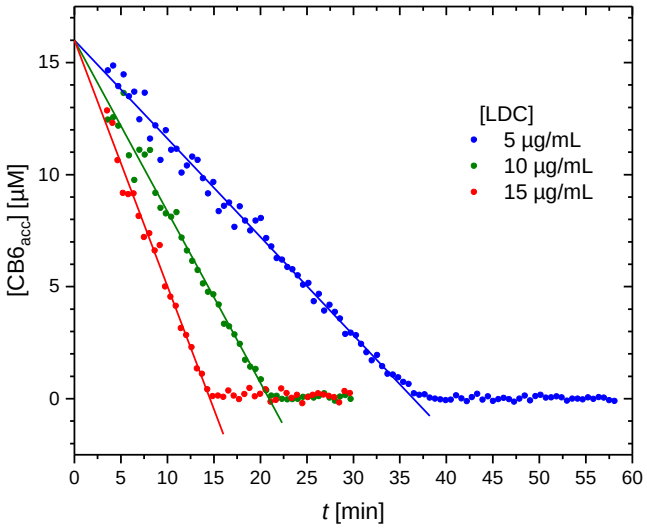

Fig. 3: Time course of the concentration of accessible CB6 as extracted from the UCS spectra displayed in Fig. 2 during the enzymatic reaction for three different concentrations of LDC and an initial CB6 concentration of 16 µM. The slope of those curves is proportional to the substrate conversion rate, as indicated by Eq. (1).

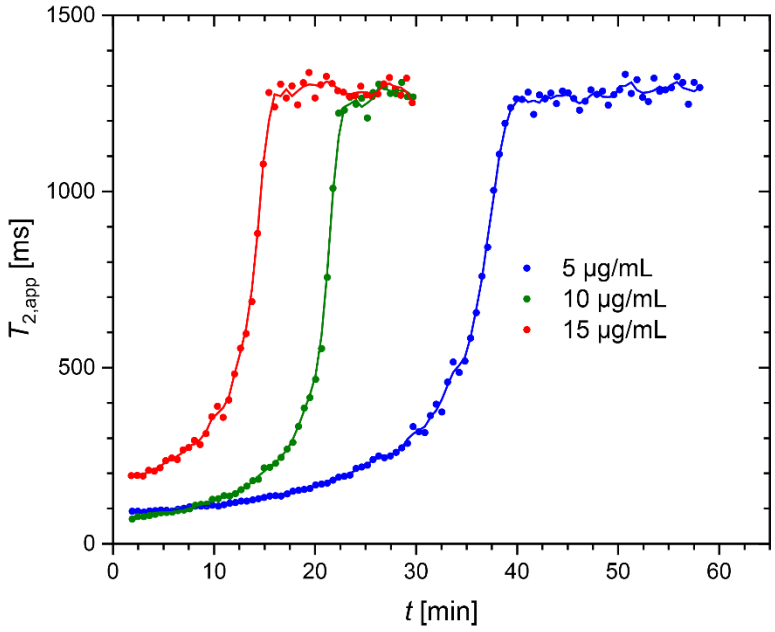

Fig. 4: Time series of the observed $T_{2,app}$ for three different concentrations of the enzyme LDC. The solid lines were obtained with an adjacent average smoothing filter (window size = 3). Analysis was then done by identifying the cut-off time for transition into the plateau with the second derivative of the smoothed data, $(d/dt)^2\ T_{2,app}\ (t_{off}) = 0$.

Time-resolved Monitoring of Enzyme Activity with Ultrafast Hyper-CEST Spectroscopy

Jörg Döpfert[1], Matthias Schnurr[1], Martin Kunth,[1*] Honor May Rose[1], Andreas Hennig[2], and Leif Schröder[1]

Chemical exchange saturation transfer with hyperpolarized Xe is used in a displacement assay to monitor the enzymatic conversion of a substrate into a product. It exploits the competitive binding of the enzymatic product on the one hand and ^{129}Xe on the other hand to a supramolecular host. We here apply a method that drastically accelerates the acquisition of Hyper-CEST spectra *in vitro* using magnetic field gradients to monitor the initial reaction rate and to derive the specific enzyme activity.